Arc dynamics of a pulsed DC nitrogen rotating gliding arc discharge

F. S. Zhu[ab], H. Zhang[a], X. D. Li[a,], A. J. Wu[a], J. H. Yan[a], M. J. Ni[a], X. Tu[b,]**

[a] State Key Laboratory of Clean Energy Utilization, Zhejiang University, Hangzhou 310027, China

[b] Department of Electrical Engineering and Electronics, University of Liverpool,

Liverpool L69 3GJ, UK

Corresponding authors*

Dr. Xin Tu

Department of Electrical Engineering and Electronics

University of Liverpool, Liverpool, L69 3GJ

UK

E-mail: xin.tu@liverpool.ac.uk

Prof. Xiaodong Li

State Key Laboratory of Clean Energy Utilization,

Zhejiang University, Hangzhou 310027,

China

E-mail: lixd@zju.edu.cn

Abstract

In this study, a novel pulsed direct current (DC) rotating gliding arc (RGA) plasma reactor co-driven by an external magnetic field and a tangential gas flow has been developed. The dynamic characteristics of the rotating gliding arc have been investigated by means of numerical simulation and experiment. The simulation results show that a highly turbulent vortex flow can be generated at the bottom of the RGA reactor to accelerate the arc rotation after arc ignition, whereas the magnitude of gas velocity declined significantly along the axial direction of the RGA reactor. The calculated arc rotation frequency (14.4 Hz) is reasonably close to the experimental result (18.5 Hz) at a gas flow rate of 10 L/min. In the presence of an external magnet, the arc rotation frequency is around five times higher than that of the RGA reactor without using a magnet, which suggests that the external magnetic field plays a dominant role in the maintenance of the arc rotation in the upper zone of the RGA reactor. In addition, when the magnet is placed outside the reactor reversely to form a reverse external magnetic field, the arc can be stabilized at a fixed position in the inner wall of the outer electrode at a critical gas flow rate of 16 L/min.

Keywords: Rotating gliding arc (RGA); arc dynamics; pulsed discharge; rotation frequency; magnetic field

1. Introduction

Gliding arc discharge (GAD) is a transitional non-equilibrium plasma with a high electron density of 10^{20}-10^{23} m^{-3} [1-3]. A typical conventional gliding arc reactor consists of two divergent electrodes. The arc is initially formed at the narrowest gap between the electrodes, and then elongated along the electrodes by the force of gas flow. The length of the gliding arc increases until its extinction unless the arc short-cuts a long current path with a shorter one. [4-8].

With the dual merits of thermal and non-thermal plasmas, GAD has attracted significant interests for methane activation [2, 9-11], CO_2 conversion [12-14] combustion enhancement [15, 16], surface treatment [17, 18] and reforming of heavy hydrocarbons [19, 20]. However, the conventional GAD systems suffer from several drawbacks which limit their industrial applications. For example, in the conventional GAD design, significant amounts of reactants do not pass the plasma arc zone due to the planar structure of the electrodes, resulting in a low conversion and efficiency. Moreover, the evolution cycle of arc ignition, elongation and extinction, occurred in conventional GAD systems leads to the formation of unstable and non-uniform plasma zone [21].

To tackle the challenges facing conventional GAD systems, different GAD configurations have been designed and developed in recent years. GAD reactors with multiple electrodes (e.g. 3 electrodes or 6 electrodes) have been developed to increase the volume of the arc region [22,23]. Gallagher et al. used a swirl generator with tangential inlets to create a gliding arc plasmatron with either a forward-vortex flow (FVF) or a reverse-vortex flow (RVF), both of which can effectively enhance the interaction between reactants and plasma discharge and minimize the electrode erosion [24,25]. Fridman et al. designed a magnetically stabilized gliding arc (MGA) reactor, using Lorentz force to keep the plasma

arc in a non-equilibrium regime [15]. We have developed a novel DC rotating gliding arc (RGA) reactor co-driven by a tangential gas flow and an external magnetic field, combining the advantages of both FVF and MGA to enlarge and stabilize the plasma region [26]. Our previous studies have shown that this novel RGA reactor could significantly enhance the conversion, product selectivity and energy efficiency in the plasma synthesis of fuels and chemicals [27-30].

Although the new designs of gliding arc systems have shown promising potential for fuel synthesis and energy conversion, their underlying characteristics are different from those of the GAD with planar electrodes and could be of primary importance for the further optimization of the plasma processes. For the RGA discharge, the independent contribution of gas flow and magnetic field on the acceleration of arc motion has not been revealed. In addition, when using a normal DC power supply, an external ballast resistor is always needed to limit the current, which consumes above 50% of the total input energy.

In this study, a custom made high voltage pulsed DC power supply has been used to generate a RGA plasma without adding an external resistor for the first time. The influence of swirling flow and external magnetic field on the arc dynamics has been investigated by combined means of numerical simulation and experiment to gain better insights into the physical properties and dynamic behavior of the pulsed RGA discharge, providing new knowledge for further scale-up and optimization of the reactor.

2. Experimental setup

Fig. 1 shows the schematic diagram of the experimental setup. The RGA reactor consists of two concentric stainless-steel electrodes. The shortest gap between the cone-shaped inner electrode (anode) and the cylindrical outer electrode (cathode) is 2 mm. A ring magnet with a magnetic flux density of 0.1 T is coaxially mounted around the outer electrode, to provide an upward magnetic field. The gas is injected through three tangential inlets at the bottom of the reactor to form a swirling flow. With the combined effects of magnetic field and vortex flow, the arc can be finally stabilized at the tip of the inner electrode and rotates rapidly, providing a wide three-dimensional plasma zone (see Fig.1). More detailed description of the RGA reactor can be found in our previous work [28].

A DC high voltage pulsed power supply (CTP-2000K, Nanjing Suman, Ltd.) is used for the generation of RGA. This power supply can output high frequency (~5 kHz) and unidirectional signals (see Fig.2), avoiding the use of external ballast resistor. In addition, high frequency periodic variation of the voltage and current can inhibit over-heating of the discharge.

The images of the arc motion are recorded by a high-speed camera (Phantom 7) with a shutter speed fixed at 5000 frames per second. The arc voltage is measured by a high-voltage probe (Tektronix P6015A), while the arc current is recorded using a current probe (Tektronix TCP303). All the electrical signals are sampled using a four-channel digital oscilloscope (Tektronix, MDO 3024). By using the trigger function of the oscilloscope, arc images and electrical signals are recorded simultaneously.

For the computational fluid dynamics (CFD) simulation, GAMBIT software is used for geometry construction and mesh generation [31]. The distributions of the gas flow field and gas velocity inside the RGA reactor are simulated and calculated using FLUENT software [32].

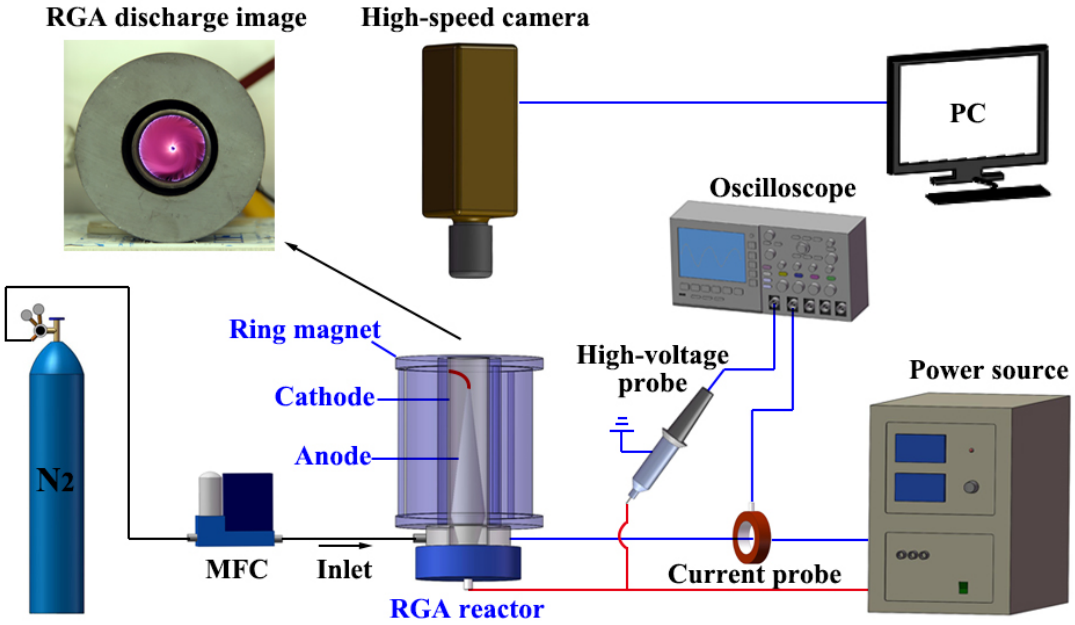

Fig. 1 Schematic diagram of the RGA experimental setup.

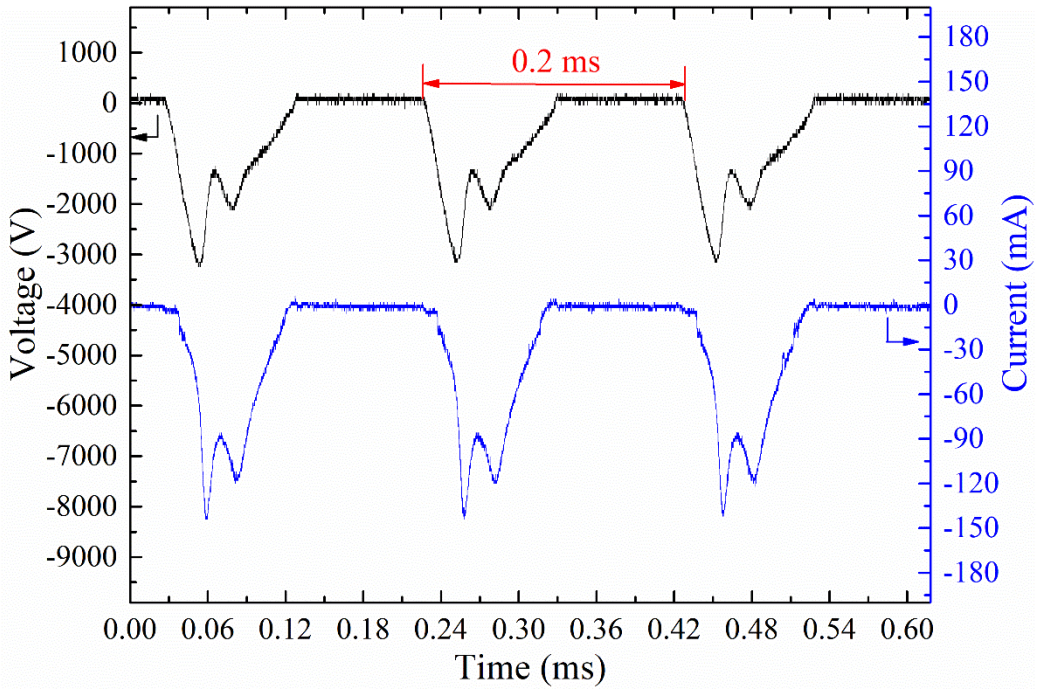

Fig. 2 Voltage and current waveforms of the RGA discharge.

3. Results and discussion

3.1 Flow field distribution

A simplified geometric model based on the configuration of the RGA reactor is developed using GAMBIT software. The central point of the outlet face is set as the coordinate origin. As shown in Fig. 3, hybrid tetrahedral and hexahedral meshes with nearly 1.1 million cells are generated. Compared to the Spalart-Allmaras (S-A) model and standard k-epsilon model, the Re-Normalization Group (RNG) k-epsilon model is more suitable for simulating a swirling flow, and thus has been selected in this simulation [33]. The model is based on the following assumptions: firstly, the gas flow inside the reactor was considered as a steady 3D and incompressible turbulent flow; secondly, the simulation was carried out in the absence of plasma discharge; thirdly, the effect of gravity on gas flow was neglected.

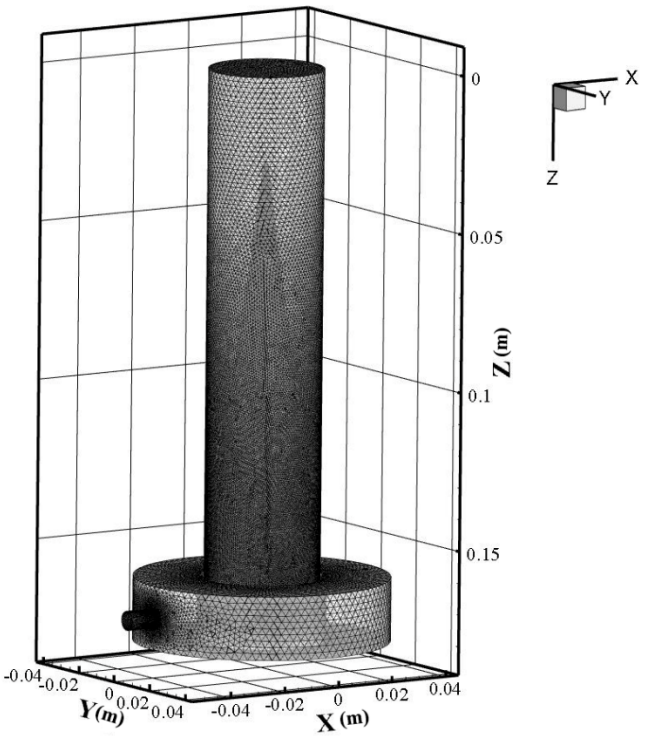

Fig. 3 Geometric model and finite elements mesh of the RGA reactor.

Fig. 4 shows the contour of the gas velocity magnitude along the axial cross section (Y=0) and the horizontal cross section (Z=170 mm) of the tangential inlets at three different flow rates. In Fig. 4 (a)-(c), the magnitude of the average velocity increases with rising input flow rate. However, the distribution of the flow field along the vertical cross section is similar regardless of the variation of flow rate. After passing the tangential inlets, the flow velocity reaches the maximum value in the bottom of the reactor. Due to the increase of the cross section of the electrode gap, the magnitude of the flow velocity is lower in the upper discharge area. Fig. 4 (d)-(f) show that a high turbulent vortex flow can be generated in the bottom of the RGA reactor through the tangential inlets (with a diameter of 2 mm). A better swirling effect at the tangential inlet plane could be achieved at a higher input flow rate. However, a higher input flow rate means a shorter residence time, which is not beneficial for the effective conversion of the reactants. On the other hand, high flow rate enhances the convection effect and consumes more energy, resulting in the instability of the discharge.

In addition, Fig. 5 shows the evolution of the velocity magnitude along Z-axis at three different flow rates. Note that we choose the midpoint (X=17 mm, Y=0 mm) of the narrowest gap to plot the velocity, since there is no flow in the region occupied by the inner electrode. The velocity decreases significantly from 0.81 m/s, 7.81 m/s and 16.16 m/s at the tangential inlet plane (Z=170 mm) to 0.0085 m/s, 0.088 m/s and 0.26 m/s at the tip plane of the inner electrode (Z=30 mm) with a flow rate of 2 L/min, 10 L/min and 18 L/min, respectively. These calculated results indicate that the gas flow has a significant effect on driving the rotation of the arc in the bottom of the reactor, due to its high velocity and strong

vortex. The effect of gas flow on arc motion decays along the axial direction of the reactor with the decrease of the velocity magnitude. At the tip of the inner electrode, where the arc is finally stabilized, the gas flow only has a weak effect on the arc rotation while the magnetic field plays a dominant role in maintaining the arc motion. The effect of magnetic field on the arc behavior is experimentally investigated in the following section.

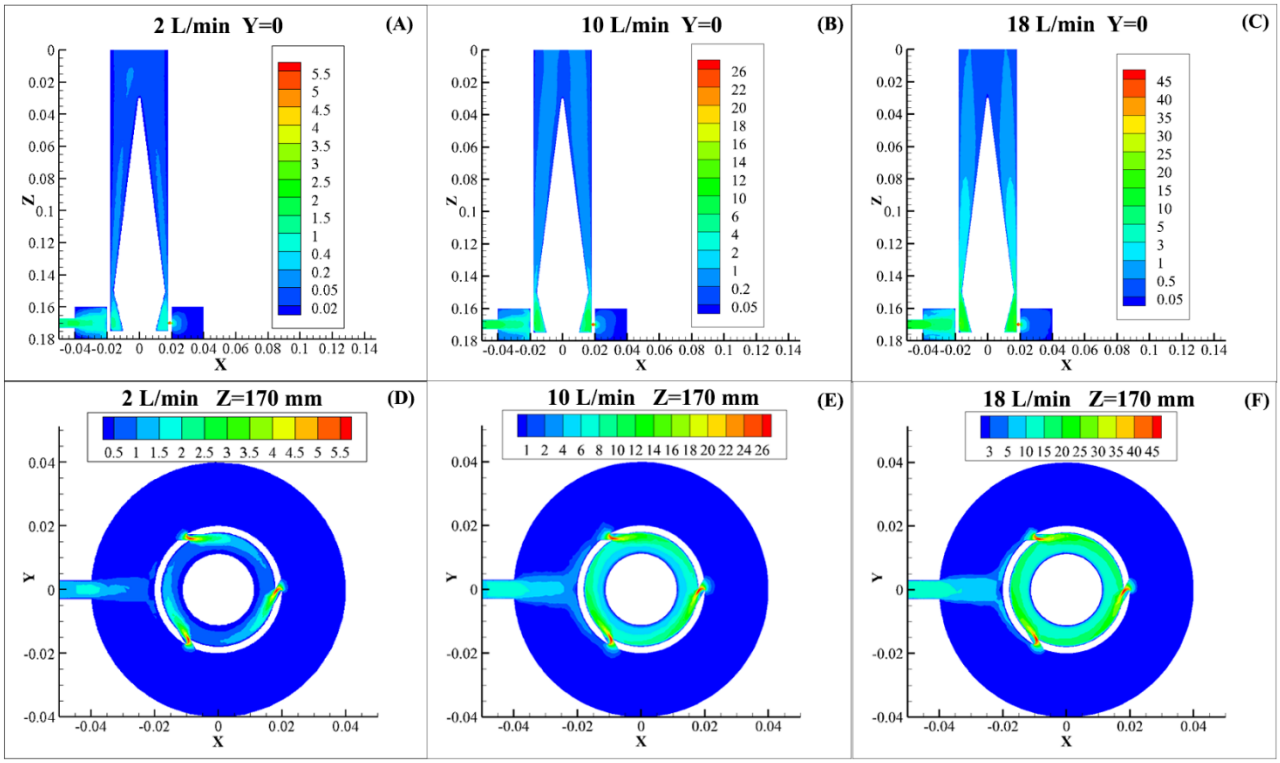

Fig. 4 Contour of gas velocity magnitude at different flow rates.

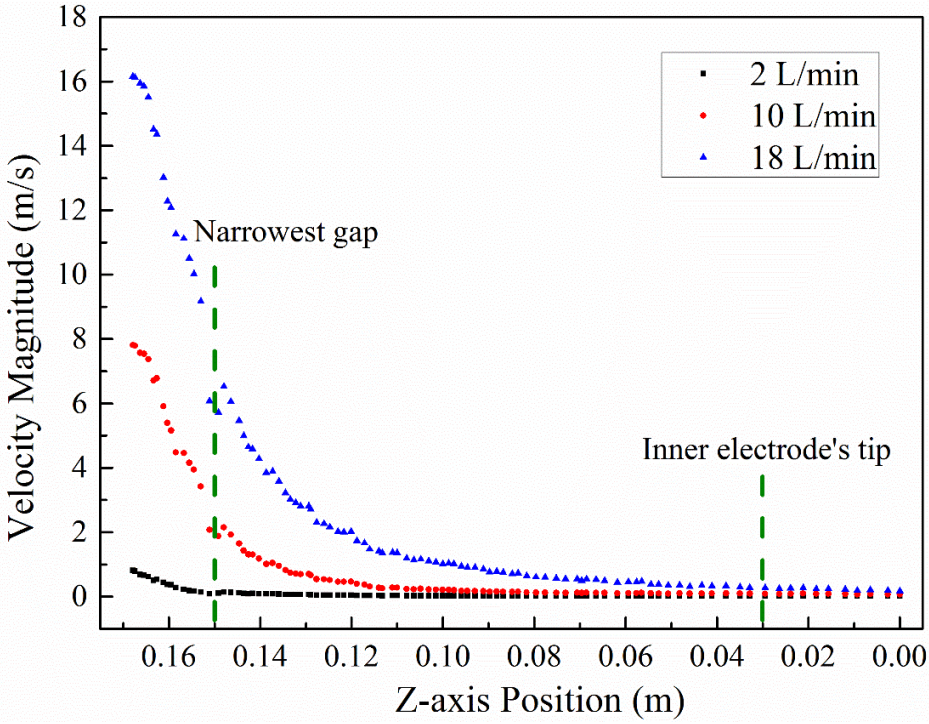

Fig. 5 Variation of velocity magnitude along Z-axis.

As described before, the plasma arc, after its ignition, will move upward and be finally anchored at the tip of the inner electrode. The tip is located at the Z=30 mm plane according to the geometric model, and the velocity distribution on this plane can provide useful information to understand the effect of gas flow on the arc motion. Since the vertical gas velocity has no effect on the acceleration of the arc rotation, here we only consider the horizontal tangential velocity. Fig. 6 shows the variation of tangential velocity along X-axis at Z=30 mm cross section with a flow rate of 10 L/min and 18 L/min. The tangential velocity at different flow rates distributes symmetrically but reaches the maximum value at different X-axis locations. The highest tangential velocity of 0.16 m/s is obtained at X=9.8 mm at a flow rate of 10 L/min, while at a flow rate of 18 L/min, the maximum velocity is 0.49 m/s at X=11 mm. The different locations of the maxima are mainly attributed to the formation of a larger centrifugal force at a higher flow rate.

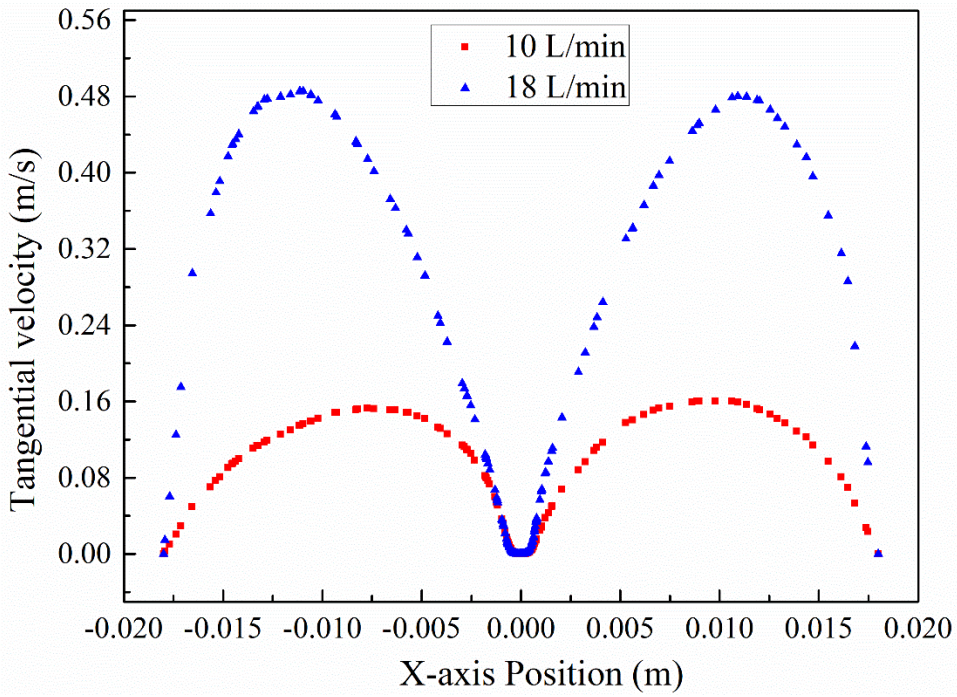

Fig. 6 Variation of tangential velocity along X-axis at Z=30 mm cross section.

3.2 Arc dynamic behavior with a magnet

Fig. 7 shows the photographs of arc motion taken by the high-speed camera. With the combined effect of swirling flow and magnetic field, the arc can rotate rapidly at a fixed period (T) of 54 ms. As the temperature of the arc column is high, the plasma has a much higher viscosity compared to the surrounding gas. According to the classic plasma string model, the arc can be simplified to a current-carrying cylinder, which is 'not transparent' to the surrounding gas [15,34,35]. There are mainly two sets of forces governing the movement of the arcs: i) Lorentz force F_L from the external magnetic field and ii) drag force F_d from the surrounding gas. These two forces per unit length on the arcs can be calculated as following equations:

$$F_L = IB \quad (1)$$

$$F_d = \frac{1}{2} C_d \rho u^2 d \quad (2)$$

$$u = u_1 - u_2 \quad (3)$$

Here, I is the arc current (~30.0 mA), B is the magnetic flux density (0.1 T), C_d is the drag coefficient, ρ is the density of nitrogen (1.138 kg/m^3), u is the arc velocity relative to the surrounding gas (u_1 is the arc velocity and u_2 is the gas velocity), and d is the arc diameter measured (~2 mm). For a smooth cylinder, the drag coefficient C_d is about 1.1 when the Reynolds number is in a 10^3 magnitude [36]. F_L=F_d is expected when the plasma arc moves in the steady state. Solving the relevant equations (Eqs. 1-3), the arc rotation frequency (f) can be calculated by:

$$f = \frac{1}{\pi D}\left(\sqrt{\frac{2IB}{C_d \rho d}} + u_2\right) \quad (4)$$

Here, D is the inner diameter of the cathode (36 mm). The calculated rotation frequency (14.4 Hz) is close to the experimental result (18.5 Hz) measured by the high-speed photography. Note that the tangential gas velocity determined from the numerical simulation is used as u_2 to calculate the arc velocity (u_1) and frequency (f) in this work. Fridman et al. [15] reported that a similar arc rotation frequency of 20 Hz in a MGA reactor at an arc current of 30 mA. According to equation (4), the arc rotation of the RGA reactor can be controlled by changing either arc current (I) or magnetic flux density (B). Recently, Zhu et al. reported a 3D method for the measurement of gas velocity (u_2) and relative velocity (slip velocity) u of a gliding arc plasma using two synchronized high-speed cameras [37]. Compared to 2D methods, they found that the 3D method is more accurate for the measurement of the slip velocity and the length of the arc column [34].

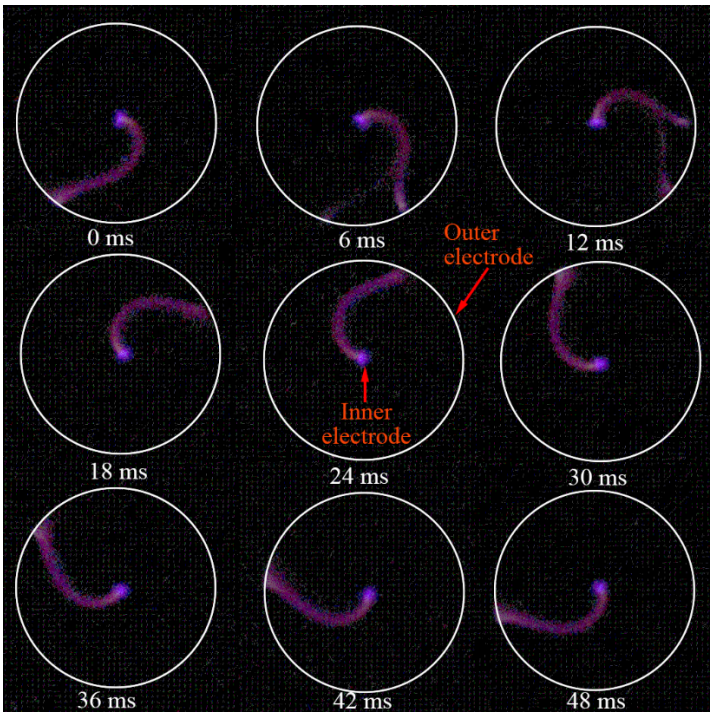

Fig. 7 Dynamic behavior of the RGA discharge in N_2

3.3 Arc dynamic behavior without a magnet

To understand the role of gas flow in the arc motion, the images of the RGA have also been recorded in the absence of the ring magnet at a gas flow rate of 10 L/min, as shown in Fig. 8. Compared to the arc rotation (18.5 Hz) in the presence of the magnet (Fig. 7), the frequency of the arc rotation without the magnet is significantly lower (4 Hz), resulted in the generation of a single arc channel instead of a successive plasma zone. This finding suggests that the external magnetic field plays a dominant role in the maintenance of the arc rotation in the upper zone of the RGA reactor. In addition, the shape and length of the plasma arc is also affected by the presence or absence of the external ring magnet. Clearly, compared to the arcs generated in the RGA reactor with the addition of the external magnet, the shape of the arcs is less curved and the arc length becomes shorter without using the magnet.

The rotation frequency of the gas (2.8 Hz) can be calculated using the equation $f=u_2/2\pi r$. Here we choose the midpoint (X=9 mm) as a massless tracer particle for the calculation and the gas tangential velocity u_2 from the simulation is 0.16 m/s. Generally, this value (2.8 Hz) should be slightly larger than the observed arc rotation frequency since there is a slip velocity between the arc and the flow [37]. However, the simulated gas rotation frequency is lower than the arc rotation frequency in this study, which means that our model might slightly underestimate the gas velocity.

Noticeably, by changing reactor configurations and operation parameters, it is possible to maintain a rapid arc velocity without adding an external magnet field. Lee et al. [38] reported three different discharge modes in a similar 3D gliding arc reactor in the absence of a ring magnet. In their studies, a wide 3D plasma zone can be formed in the steady discharge mode. However, this mode can only be achieved at a relatively high input power (above 400 W) and high gas flow rates (10-20 L/min) in a compact plasma reactor (inner diameter: 25 mm; height: 90 mm). Based on their results and the velocity distribution along the reactor axis, the effect of gas drag force on the arc rotation is expected to be enhanced by reducing the reactor height in the future design. But compared to the effect of swirling gas, the Lorentz force is more important for governing the arc rotation at its anchored position, especially when the flow rate is low (e.g. 2 L/min).

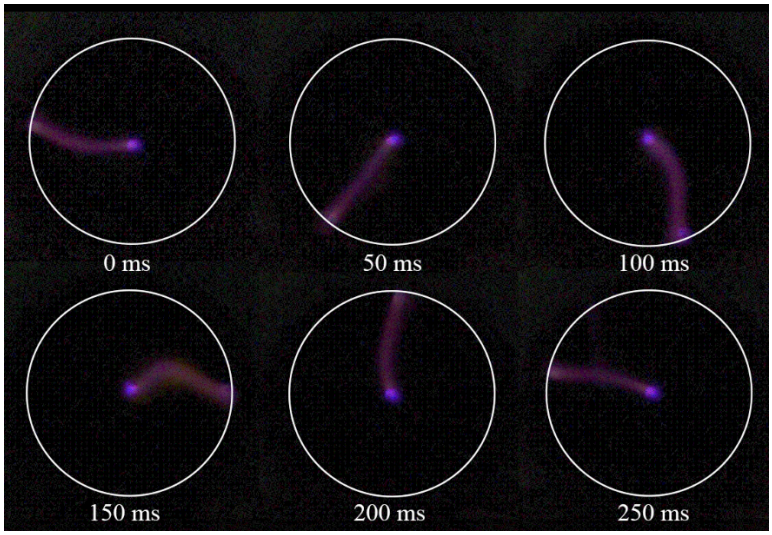

Fig. 8 Dynamic behavior of the RGA discharge without a magnet.

3.4 Arc dynamic behavior with a reverse magnet

In this section, the ring magnet is placed outside the RGA reactor reversely to form a reverse magnetic field, providing a Lorentz force opposite to the tangential gas flow. The arc moves in the direction of Lorentz force at a low gas flow rate, while the arc rotation frequency decreases with the increase of the gas flow rate and finally turns to zero at a critical gas flow rate when the gas drag force is equal to the Lorentz force. In this work, this critical gas flow rate is 16 L/min. Fig. 9 shows the images of arc motion as well as the direction of Lorentz force and swirling flow at a flow rate of 16 L/min. It can be seen that the arc is stabilized between the tip of the inner electrode and a fixed point in the inner wall of the outer electrode. With the evolution of time, the arc is slightly twisted but does not rotate any more. The arc can rotate again when further increasing the gas flow rate, following the direction of the gas drag force. These interesting phenomena could provide new insights into arc dynamics for the better control of the arc motion.

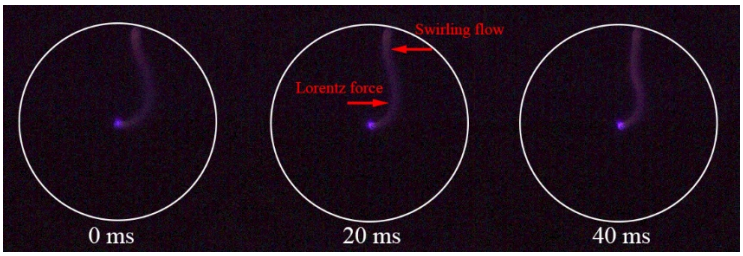

Fig. 9 Dynamic behavior of the RGA discharge with a reverse magnet.

4. Conclusion

The characteristics of a pulsed DC rotating gliding arc plasma have been investigated by numerical simulation and experiment. The calculated arc rotation frequency agrees well with the actual frequency.

At the bottom of the reactor, high velocity and strong vortex after the gas coming from the tangential inlets can be achieved. However, the value of the velocity decreases dramatically from 0.81 m/s, 7.81 m/s and 16.16 m/s at the tangential inlets plane to 0.0085 m/s, 0.088 m/s and 0.26 m/s at the inner electrode's tip plane with a flow rate of 2 L/min, 10 L/min and 18 L/min, respectively.

In the presence of the magnet, the arc rotation frequency (18.5 Hz) is 4.6 times higher than that (4 Hz) obtained without the magnet, which implies that the magnetic field plays a dominant role in maintaining the arc rotation in the upper zone of the reactor. In the case of reverse magnet, a critical value of gas flow rate at 16 L/min is found, under which the arc will be stabilized between two fixed points.

Acknowledgement

The support of this work by the National Natural Science Foundation of China (No. 51576174, No.

51706204), EPSRC SUPERGEN Bioenergy Challenge Programme (No. EP/M013162/1), EPSRC Impact Acceleration Account (IAA) and ODA Research Seed funding is gratefully acknowledged. Fengsen Zhu acknowledges the support by China Scholarship Council (CSC), Newton Fund and British Council (UK-China PhD Placement Grant).

References:

[1] Fridman A 2008 *Plasma chemistry* Cambridge university press.

[2] Tu X and Whitehead J 2014 *Int. J. Hydrogen Energy* **39** 9658-69.

[3] Trenchev G, Kolev S and Bogaerts A 2016 *Plasma Sources Sci. Technol.* **25** 35014.

[4] Fridman A, Nester S, Kennedy L, Saveliev A and Mutaf-Yardimci O 1999 *Progress Energy Combust. Sci.* **25** 211-31.

[5] Tu X, Gallon H J and Whitehead J C 2011 *IEEE Trans. Plasma Sci.* **39** 2900-1.

[6] Tu X, Yu L, Yan J H, Cen K F and Chéron B G 2009 *Physics of Plasmas* **16** 113506.

[7] Sun Z, Zhu J, Li Z, Aldén M, Leipold F, Salewski M and Kusano Y 2013 *Optics Express* **21** 6028-44.

[8] Zhu J, Sun Z, Li Z, Ehn A, Aldén M, Salewski M, Leipold F and Kusano Y 2014 *J. Phys. D: Appl. Phys.* **47** 295203.

[9] Indarto A, Choi J, Lee H and Song H 2006 *Energy* **31** 2986-95.

[10] Pacheco J, Soria G, Pacheco M, Valdivia R, Ramos F, Frías H, Durán M and Hidalgo M 2015 *Int. J. Hydrogen Energy* **40** 17165-71.

[11] Kang H, Lee DH, Kim K, Jo S, Pyun S, Song Y and Yu S 2016 *Fuel Process. Technol.* **148** 209-16.

[12] Wang W, Berthelot A, Kolev S, Tu X and Bogaerts A 2016 *Plasma Sources Sci. Technol.* **25** 65012.

[13] Indarto A, Choi J, Lee H and Song H 2006 *Environ. Eng. Sci.* **23** 1033-43.

[14] Wang W, Mei D, Tu X and Bogaerts A 2017 *Chem. Eng. J.* **330** 11-25.

[15] Fridman A, Gutsol A, Gangoli S, Ju Y and Ombrello T 2008 *J. Propulsion Power* **24** 1216-28.

[16] Sun W, Uddi M, Won S, Ombrello T, Carter C and Ju Y 2012 *Combust. Flame* **159** 221-9.

[17] Kusano Y, Norrman K, Drews J, Leipold F, Singh S V, Morgen P, Bardenshtein A and Krebs N 2011 *Surf. Coat. Technol.* **205** S490-4.

[18] Kusano Y, Sorensen B F, Andersen T L, Toftegaard H L, Leipold F, Salewski M, Sun Z W, Zhu J J, Li Z S and Alden M 2013 *J. Phys. D: Appl. Phys.* **46** 135203.

[19] Liu S, Mei D, Wang L and Tu X 2017 *Chem. Eng. J.* **307** 793-802.

[20] Yu L, Li X, Tu X, Wang Y, Lu S and Yan J 2009 *J. Phys. Chem. A* **114** 360-8.

[21] Zhang C, Shao T, Xu J, Ma H, Duan L, Ren C and Yan P 2012 *IEEE Trans. Plasma Sci.* **40** 2843-9.

[22] Chun Y, Yang Y and Yoshikawa K 2009 *Catal. Today* **148** 283-9.

[23] Baba T, Takeuchi Y, Stryczewska H and Aoqui S 2012 *Przegląd Elektrotechniczny* **88** 86-8.

[24] Gallagher M J, Geiger R, Polevich A, Rabinovich A, Gutsol A and Fridman A 2010 *Fuel* **89** 1187-92.

[25] Nunnally T, Gutsol K, Rabinovich A, Fridman A, Gutsol A and Kemoun A 2011 *J. Phys. D: Appl. Phys.* **44** 274009.

[26] Zhang H., Li X D, Zhang Y Q, Chen T, Yan J H and Du C M 2012 *IEEE Trans. Plasma Sci.* **40** 3493-8.

[27] Zhang H, Li X, Zhu F, Cen K, Du C and Tu X 2017 *Chem. Eng. J.* **310, Part 1** 114-9.

[28] Zhu F, Li X, Zhang H, Wu A, Yan J, Ni M, Zhang H and Buekens A 2016 *Fuel* **176** 78-85.

[29] Zhu F, Zhang H, Yang J, Yan J, Ni M and Li X 2017 *Chem. Letters* **46** 1341-3.

[30] Zhu F, Zhang H, Yan X, Yan J, Ni M, Li X and Tu X 2017 *Fuel* **199** 430-7.

[31] Fluent I. 2004 *Gambit 2.4 tutorial guide*.

[32] Fluent I. 2006 *Fluent documentation*.

[33] Escue A and Cui J 2010 *Appl. Math. Model.* **34** 2840-9.

[34] Richard F, Cormier J M, Pellerin S and Chapelle J 1996 *J. Appl. Phys.* **79** 2245-50.

[35] Pellerin S, Richard F, Chapelle J, Cormier J M and Musiol K 2000 *J.Phys. D: Appl. Phys.* **33** 2407.

[36] Munson B R, Young D F and Okiishi T H 1990 *New York* **3**.

[37] Zhu J, Gao J, Ehn A, Aldén M, Li Z, Moseev D, Kusano Y, Salewski M, Alpers A and Gritzmann P 2015 *Appl. Phys. Letters* **106** 44101.

[38] Lee D H, Kim K T, Cha M S and Song Y H 2007 *Proceed. Combust. Inst.* **31** 3343-51.